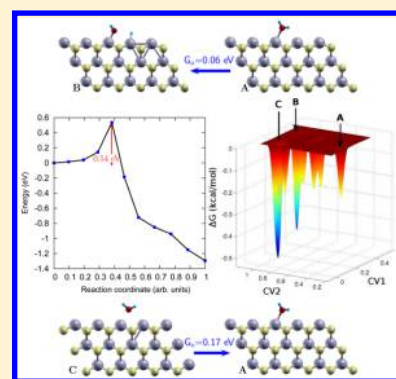# Adsorption and Dissociation of H_2O on Monolayered MoS_2 Edges: Energetics and Mechanism from *ab Initio* Simulations

Kulbir Kaur Ghuman, Shwetank Yadav, and Chandra Veer Singh*

Department of Materials Science and Engineering, University of Toronto, 184 College Street, Suite 140, Toronto, ON M5S 3E4, Canada

Ⓢ *Supporting Information*

ABSTRACT: The dissociation of water on 2D monolayer molybdenum disulfide (MoS_2) edges was studied with density functional theory. The catalytically active sites for H_2O, H, and OH adsorption on MoS_2 edges with 0% (Mo-edge), 50% (S50-edge), and 100% (S100-edge) sulfur coverage were determined, and the Mo-edge was found to be the most favorable for adsorption of all species. The water dissociation reaction was then simulated on all edges using the climbing image nudged elastic band (CI-NEB) technique. The reaction was found to be endothermic on the S100-edge and exothermic for the S50- and Mo-edges, with the Mo-edge having the lowest activation energy barrier. Water dissociation was then explored on the Mo-edge using metadynamics biased *ab initio* molecular dynamics (AIMD) methods to explore the reaction mechanism at finite temperature. These simulations revealed that water dissociation can proceed by two mechanisms: the first by splitting into adsorbed OH and H species produced a particularly small activation free energy barrier of 0.06 eV (5.89 kJ/mol), and the second by formation of desorbed H_2 and adsorbed O atom had a higher activation barrier of 0.36 eV (34.74 kJ/mol) which was nevertheless relatively small. These activation barrier results, along with reaction rate calculations, suggest that water dissociation will occur spontaneously at room temperature on the Mo-edge.

1. INTRODUCTION

The water dissociation reaction is a fundamentally important process not only for renewable generation of hydrogen fuel from water through the hydrogen evolution reaction (HER) but also because it plays an important role in various other reactions, such as water-gas shift (WGS, $CO + H_2O \rightarrow CO_2 + H_2$) reaction. Because of the high energetic costs of water splitting, there are many catalyst materials currently under investigation to facilitate the process.[1−3] One such class of materials includes transition metal chalcogenides—compounds consisting of chalcogen (elements in group 16 of the periodic table such as oxygen and sulfur) anions and transition metal cations. Various theoretical and experimental studies have reported the synthesis and investigated the properties of chalcogenide MX_2 monolayers, such as MoS_2, WS_2, $MoSe_2$, $MoTe_2$, TiS_2, TaS_2, $TaSe_2$, $NiTe_2$, and ZrS_2, attracting significant attention for a broad range of applications including electronics, optoelectronics, photovoltaics, and photocatalysis.[4−10] Reducing the dimension from 3D to 2D leads to change in the structural, electronic, and vibrational properties of these materials. For example, a comparative study of lattice dynamics of 3D and 2D MoS_2 shows that absence of a weak inter layer interaction in 2D single-layer MoS_2 results in the softening of some of the Raman-active modes.[11] As two-dimensional (2D) materials, they possess a high specific surface area ideal for catalysis and a small band gap which allows them to be strong visible light absorbers and possibly promote photocatalytic reactions.[12] In fact, both MoX_2 and WX_2 have indirect band

gaps as bulk materials while their monolayers possess direct band gaps,[13,14] highlighting the interesting properties of 2D materials. Furthermore, among these monolayers, only molybdenum disulfide (MoS_2) has its band positions aligned with the water oxidation and reduction potentials,[4] which combined with its stability against photocorrosion[15] makes it an interesting material for use as a photocatalyst for water splitting.

MoS_2 itself has been previously studied for potential applications as an electrocatalyst for hydrogen evolution. While large-scale bulk MoS_2 is a poor catalyst,[16] nanoparticles of MoS_2 have shown high HER activity.[17−20] The HER activity for these nanoparticles is strongly associated with exposed edge sites that have a local stoichiometry, physical structure, and electronic structure that differs from the catalytically inert basal planes of MoS_2.[21−23] Similar investigations are critical for designing and developing 2D MoS_2-based catalytic materials. A recent theoretical study reported that, similar to the inert basal planes of bulk MoS_2, the surface of pristine 2D MoS_2 is not very favorable for water adsorption and dissociation due to the repulsive interaction between free H_2O and the perfect surface.[24] The study looked at triple vacancy defects as a way of disrupting the perfect surface which lead to exothermic adsorption and dissociation of water molecules. However, despite the excellent activity of MoS_2 nanoparticle edges, the
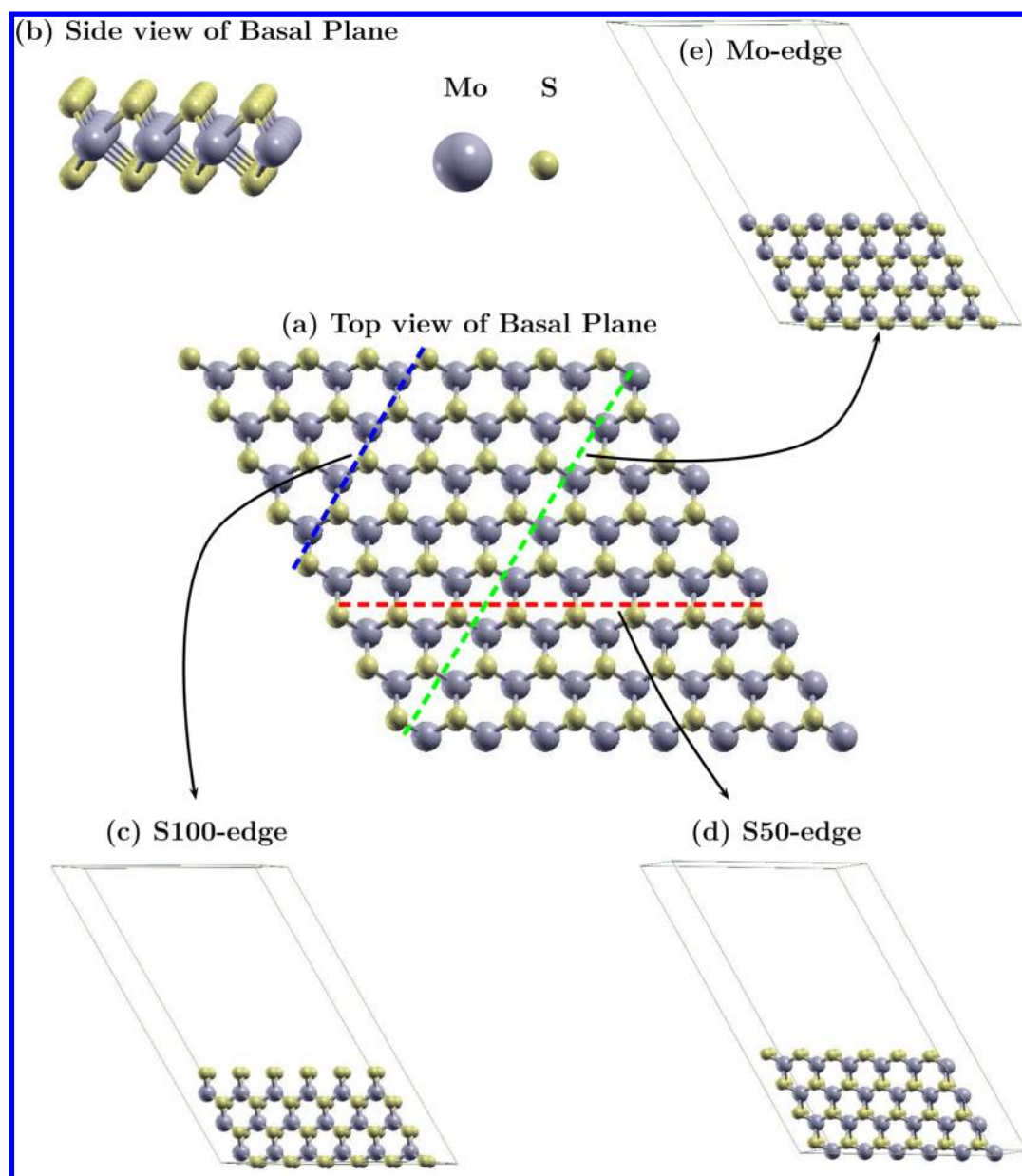
Figure 1. (a) Top and (b) side view of the perfect basal plane of 2D MoS$_2$. Blue, red, and green dotted lines show the location of the three most thermodynamically stable surface terminations. These terminations, along with the their simulation supercells, are shown in the following: (c) S-edge with 100% (S100-edge) sulfur coverage, (d) S-edge with 50% (S50-edge) sulfur coverage, and (e) S-edge with 0% (Mo-edge) sulfur coverage. The yellow and the purple spheres represent S and Mo atoms, respectively.

hydrogen evolution reaction at room temperature has not been investigated on the three thermodynamically stable edges reported by Raybaud et al.[25] Water dissociation, as part of the WGS reaction, has only been previously investigated on two of these edges which have undergone sulfur reconstruction at high temperature and H$_2$S pressure conditions[26−28] As the water dissociation step has been suggested to be the rate-limiting step for hydrogen production for a variety of metals,[29−32] we chose to study this process on 2D MoS$_2$ edges.

This paper conducted a first-principles based in-depth investigation of water adsorption and dissociation (H$_2$O → OH$^-$ + H$^+$) mechanisms, in terms of thermodynamic stability, active sites, activation barriers, and rates of reactions on various 2D MoS$_2$ edges. First, the geometries and active sites for water adsorption were studied for three edge terminations of MoS$_2$. Next, the activation energies for the water dissociation reaction

on each edge were determined using the climbing image nudged elastic band (CI-NEB) methodology. Finite temperature effects were subsequently analyzed through *ab initio* molecular dynamics (AIMD) and metadynamics to study the water dissociation reaction on the most favorable edge. Finally, a ground state study was conducted to study OH dissociation, H migration, and H$_2$ desorption after water dissociation.

2. COMPUTATIONAL METHODS AND MODELS

2.1. *Ab Initio* Techniques. In order to understand the electronic structure and photocatalytic properties of MoS$_2$, density functional theory (DFT) was utilized. The Quantum Espresso[33] software package using the plane-wave basis set approach was utilized throughout this study. Interactions between the valence electrons and the ionic core were represented by the projector augmented wave (PAW)[34]
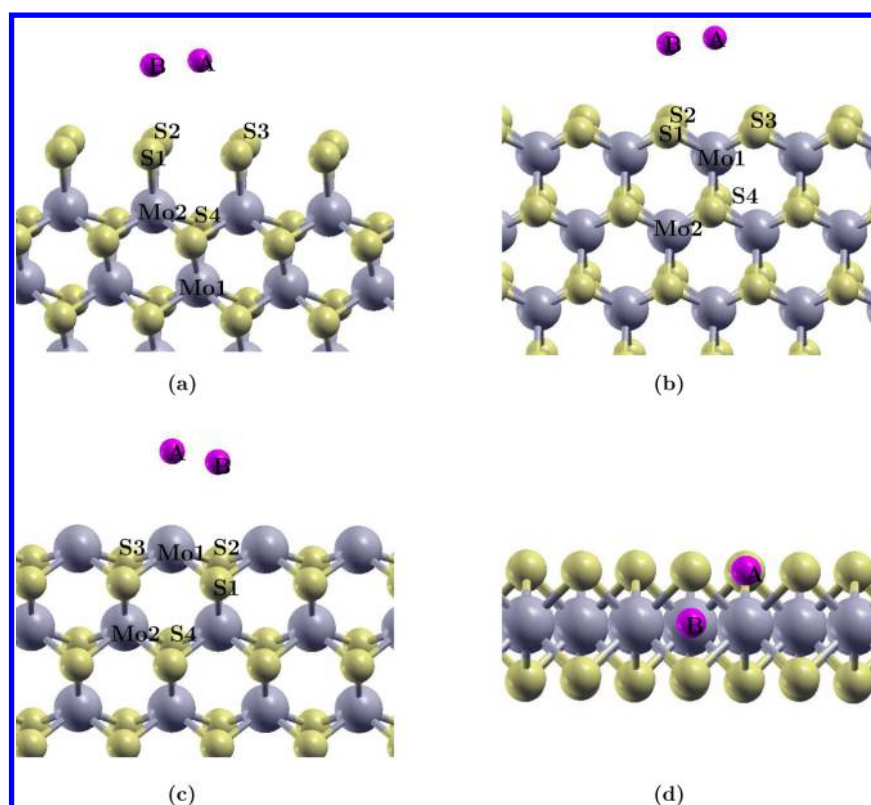
Figure 2. Sites investigated for H, OH, and H_2O adsorption on (a) S100-edge, (b) S50-edge, and (c) Mo-edge. The view of the edge with the MoS_2 plane oriented perpendicular to the page is shown in (d) with sites A and B. Mo atoms are in purple, S atoms are in yellow, and sites A and B are represented by pink spheres.

method with Perdew–Burke–Ernzerhof (PBE) formulation.[35] Kinetic energy cutoffs of 680 and 6800 eV were used for the wave functions and the charge density, respectively. Brillouin zone integrations were performed using a Monkhorst–Pack[36] grid of $4 \times 4 \times 1$ k-points, and all calculations were non-spin-polarized. A vacuum layer larger than or equivalent to 15 Å was added to avoid interaction between adjacent images. Results for system relaxations were checked for convergence with respect these parameters. Long range nonlocal effects such as van der Waals (vdW) forces were taken into account by applying van der Waals corrections through the vdW-DF2 functional.[37] The structures were relaxed using a conjugate gradient minimization algorithm until the magnitude of the residual Hellman–Feynman force on each atom was less than 0.025 eV Å^{-1}.

The evaluation of minimum-energy reaction paths (MEPs) and transition states (TS) was performed using the climbing image nudged elastic band (CI-NEB) method.[38−40] Finite temperature analysis of the system at 300 K was conducted through *ab initio* molecular dynamics (AIMD) on the Born–Oppenheimer surface which maintained temperature through the Andersen thermostat. A time step of 2.5 fs was employed for the AIMD runs, wherein Brillouin zone integrations were performed on the Γ point in order to decrease simulation times. Biased AIMD simulations were conducted using the metady-namics[41,42] technique applied through the PLUMED[43] plug-in. The biased simulations were also conducted at 300 K and initially employed a 2.5 fs time step in order to sample the overall free energy surface and then employed a 1.25 fs time step to sample specific regions of this surface with finer detail.

2.2. Structure Model. The basal plane of 2D MoS_2 consists of two hexagonal planes of sulfur (S) atoms and an intercalated

hexagonal plane of molybdenum (Mo) atoms bonded to the S atoms in a trigonal prismatic arrangement, as indicated in Figure 1a,b. A single MoS_2 sheet cut along the dotted lines (Figure 1a) is terminated by three different 1D edge terminations as shown in Figure 1c−e. The first edge termination consists of two S atoms per Mo atom representing 100% S coverage (S100-edge) shown in Figure 1c, the second consists of single S atoms representing 50% S coverage (S50-edge) shown in Figure 1d, and finally the third edge consists of Mo atoms only representing 0% S coverage (Mo-edge) as shown in Figure 1e. The supercells of basal plane, S50-edge, S100-edge, and Mo-edge consist of 48, 72, 66, and 72 atoms, respectively. The present study was restricted to these sulfur coverages as previous slab calculations[25] indicate that only these coverages are thermodynamically stable. In agreement with previous studies,[25] the S100-edge exhibits S2 dimers after relaxation and the outer Mo atoms are 6-fold-coordinated. Furthermore, it should be noted that a slight pairing of the S2 dimers is observed. Reducing the S coverage to 50% leads to a zigzag configuration for the S50-edge, where the S monomers are in a bridging position and the Mo atoms again have 6-fold coordination. The Mo-edge undergoes reconstructions due to the very low coordination (2-fold) of the Mo atoms.

3. RESULTS AND DISCUSSION

3.1. Adsorption of H, OH, and H_2O on MoS_2 Edges. As a first step, active sites for the adsorption of the H_2O, OH, and H species on each of the three chosen MoS_2 edges were investigated. A water coverage of 0.25 ML (i.e., one water molecule per unit cell) was used. The adsorption energy of an adsorbate on the surface was calculated as

$$\Delta H_{ads} = E_{tot} - E_{bare} - E_{ad} \tag{1}$$

where E_{tot} (E_{bare}) is the energy of the slab with (without) adsorbate and E_{ad} is the energy of the isolated adsorbate species calculated in the same supercell. Hence, a negative ΔH_{ads} indicates stable adsorption whereas a positive value indicates unstable adsorption. To check the performance of the edge terminations, we first investigated the possibility of water dissociation on the stoichiometric 2D MoS$_2$ surface (basal plane). We considered various high-symmetry sites and found that the water molecule possessed a positive adsorption energy and stayed away from the surface. This indicates a repulsive interaction between free H$_2$O molecule and the perfect surface of MoS$_2$ monolayer. The ΔH_{ads} values for H and OH adsorption were also found to be positive, suggesting that water dissociation will not take place on the MoS$_2$ basal plane. This is likely because the O atom cannot receive sufficient electrons in order to release H and is in agreement with previous work[24] where the layer of S atoms in the perfect nonterminated structure were observed to be repulsive to the O atom.

Next, the adsorption of H, OH, and H$_2$O on the three MoS$_2$ edges was investigated. Although each edge had different surface configurations, they were all composed of the same basic structural pattern and thus had similar types of adsorption sites. These common adsorption site types are shown in Figure 2a for the S50-edge, Figure 2b for the S100-edge, and Figure 2c for the Mo-edge. They consisted of the following: (1) on top of a S atom (marked S1), (2) on top of a Mo atom (marked Mo1), (3) a bridge site (labeled A) between two S atoms (marked S2 and S3), (4) above a S atom (marked S4), (5) a bridge site (labeled B) between two S atoms (marked S1 and S2), and (6) above a Mo atom (marked Mo2). In Figure 2d a different perspective further displays the two bridge sites.

Table 1 gives the most stable adsorption energies and sites for each species on the three edges and also contains the corresponding structural parameters. It was found that the H$_2$O molecule was energetically most stable on top of a Mo atom (marked Mo1) for both S100-edge and Mo-edge whereas it was most stable at site A for S50-edge. For all the edges, the water molecule oriented itself so as to have the O atom closest to the

MoS$_2$ surface with the H atoms facing away from the surface as seen in Figure 3. The O−H bond lengths for each edge surface were slightly larger than that of a free H$_2$O molecule (0.958 Å) in vacuum, indicating the O−H bond gets weakened when the molecule is adsorbed on MoS$_2$ edges.

The H$_2$O molecule demonstrated a stable negative adsorption energy only on the Mo-edge, while both the S100-edge and S50-edge produced positive adsorption energies unfavorable to adsorption. Among these edge terminations, only the Mo-edge has undercoordinated atoms (2-fold-coordinated surface Mo atoms) compared to the basal plane, and hence they are more likely to interact with adsorbate species. Furthermore, sites above Mo atoms were more favorable than those above S atoms as the Mo−O electronegativity difference is greater than that for S−O. Another factor which likely affected adsorbate binding ability relates to geometrical constraints. For the Mo-edge surface, the Mo1 site atoms are well exposed in isolation, allowing free interaction with the H$_2$O molecule, whereas access to Mo atoms for the S100-edge and S50-edge is blocked by S atoms to a certain degree. It should be noted that even for the Mo-edge, although there is adsorption and attraction between the H$_2$O molecule and surface, the adsorption energy is still weaker than typical covalent bond energies (for example, the bond energy of O−H bond in water is about 5.0 eV).

The electrostatic interactions between the H$_2$O molecule and edge surfaces were further confirmed by Bader charge analysis for the best adsorption sites. Charge analysis was focused on the atoms of the H$_2$O molecule and the nearest surface atoms at the adsorption location, with detailed quantitative values provided in the Supporting Information. The S and O atoms in all systems had negative effective charges, while the Mo and H atoms had positive effective charges. This helps to explain the previously noted repulsion between the O atom in the H$_2$O molecule and surface S atoms, whereas surface Mo atoms attract the O atom. This is one reason that the pristine MoS$_2$ surface does not strongly interact with H$_2$O molecules as the layer of negatively charged S atoms shields the inner Mo atoms. For the two S-edges, the S and O atoms seemed to push charge away from each other after adsorption, transferring charge to H atoms or surrounding Mo atoms, respectively. The S100-edge displayed a greater charge redistribution than S50-edge, and there appears to be a slight charge transfer to the H$_2$O molecule which ends up with a small negative overall charge. For the Mo-edge, the surface Mo atom becomes more positive and the O atom becomes more negative; this edge displays the greatest charge redistribution and polarization of the H$_2$O molecule. However, there does not seem to be a transfer of charge from Mo to O as the overall charge on the H$_2$O molecule remains zero. Hence, the adsorption of the H$_2$O molecule on Mo-edge appears to take place through induced electrostatic attraction.

In order to further study the interaction between the H$_2$O molecule and edge terminations and any possible charge transfer, we plotted the charge density difference $\Delta\rho$ for the best adsorption site on each edge as shown in Figure 3. Here $\Delta\rho = \rho(\text{edge} + H_2O) - \rho(\text{edge}) - \rho(H_2O)$, where $\rho(\text{edge} + H_2O)$ and $\rho(\text{edge})$ are the charge densities of the edge with and without adsorbed H$_2$O, respectively, and $\rho(H_2O)$ is the charge density of the isolated H$_2$O molecule. The greatest charge redistribution occurs for the Mo-edge, indicating a strong interaction between the H$_2$O molecule and nearest-neighboring Mo atom. Both the O and Mo atoms seem to be polarized, pointing to a electrostatic attraction between them as proposed
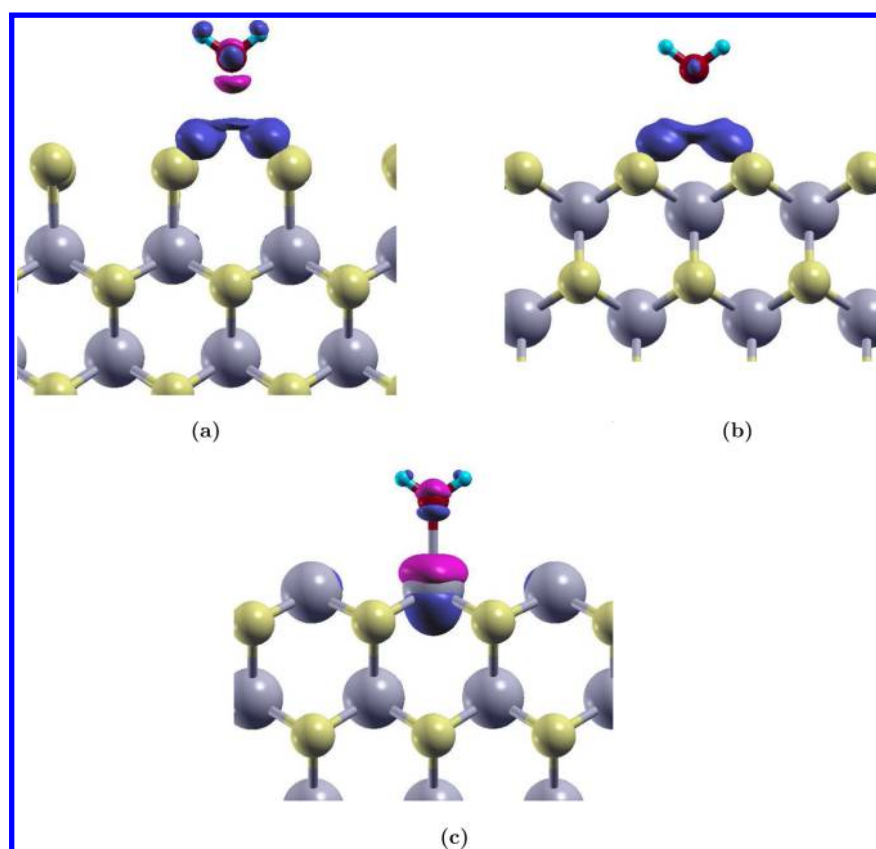
Table 1. Calculated Structural Parameters and Adsorption Energies of H$_2$O, OH, and H for the Most Stable Site on S100-Edge, S-50-Edge, and Mo-Edge[a]

most stable species	H_{ads} (eV)	h (Å)	d_{O-H}	α_{HOH}
		S100-edge		
H$_2$O (on site Mo1)	0.15	2.989	0.9796, 0.9797	103.85
OH (on site S1)	−0.215	0.251	0.988	
H (on site S1)	−0.155	0.206		
		S50-edge		
H$_2$O (on site A)	0.23	2.848	0.9783, 0.9838	103.55
OH (on site S1)	−0.275	1.682	0.995	
H (on site S1)	−0.199	1.304		
		Mo-edge		
H$_2$O (on site Mo1)	−0.55	2.274	0.9905, 0.9768	108.82
OH (on site B)	−3.863	1.630	0.983	
H (on site B)	−4.921	1.346		

[a]H_{ads} (eV) represents the adsorption energy, h (Å) represents the vertical height of the H$_2$O, OH, and H species from the surface, d_{O-H} represents the OH bond lengths for OH and H$_2$O molecules, and α_{HOH} represents the H−O−H angle for H$_2$O molecule.

Figure 3. Isosurfaces of the charge density difference $\Delta\rho$ for H_2O molecule adsorbed on the most stable site for (a) S100-edge, (b) S50-edge, and (c) Mo-edge. The purple, yellow, blue, and red spheres are Mo, S, H, and O atoms, respectively. The positive and negative isosurfaces are in pink and blue, indicating regions of charge gain and loss, respectively.

earlier. The increase in negative charge below the Mo atom, away from the surface as opposed to, further confirms that there is likely no charge transfer from the Mo atom to the O atom and is consistent with earlier Bader analysis. The large regions of charge loss between the H_2O molecule and the nearest two S atoms for the two S-edges point to the repulsion felt between the O and S atoms. On all the edges the charge gets redistributed within the H_2O molecule, indicating there is at least some level of interaction for each system.

Unlike H_2O, both H and OH species were able to stably adsorb with negative adsorption energies on all the studied edges (Table 1), which was expected as the latter two are no longer part of the stable water molecule. The most stable adsorption position for both species on the S-edges was on an S atom (marked S1 in Figure 2a,b) while it was at the bridge site B for both species on the Mo-edge (Figure 2c). For the two S-edges, OH had a stronger adsorption energy than the H atom, while the H atom had stronger adsorption for the Mo-edge. Furthermore, the adsorption energies for the Mo-edge are significantly stronger than for S-edges and are in the range of typical covalent bond energies. Hence, both H and OH seemed to have formed covalent bonds on the Mo-edge due to the strong adsorption energies and the fact that they seem to be equally spaced between adjacent Mo atoms which suggests a charge sharing arrangement.

3.2. Dissociation of H_2O on MoS_2 Edges. For the water dissociation reaction on the three studied monolayer MoS_2 edges, we performed NEB calculations with 11 images in order to evaluate the MEP and the TS energy. For each edge, the initial state (IS) and final state (FS) were obtained from the

adsorption simulations discussed in section 3.1, with the IS corresponding to H_2O adsorption (whole water molecule) and the FS corresponding to OH and H adsorption (dissociated water molecule). Figures 4, 5, and 6 present the energy profiles that represent MEP between IS and FS for S100-edge, S50-edge, and Mo-edge, respectively, along with their IS, TS, and FS geometries and activation energy barriers. The chosen TS configuration corresponds to the highest energy point along the
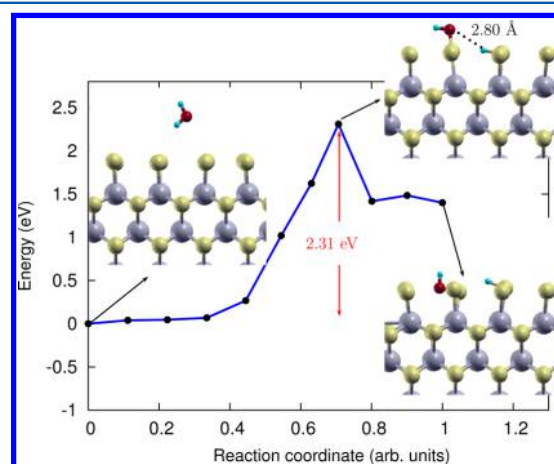

Figure 4. Reaction pathway and reaction barrier of single water dissociation on S100-edge from climbing image nudged elastic band (CI-NEB) simulation. Purple atoms represent Mo; yellow atoms represent S.
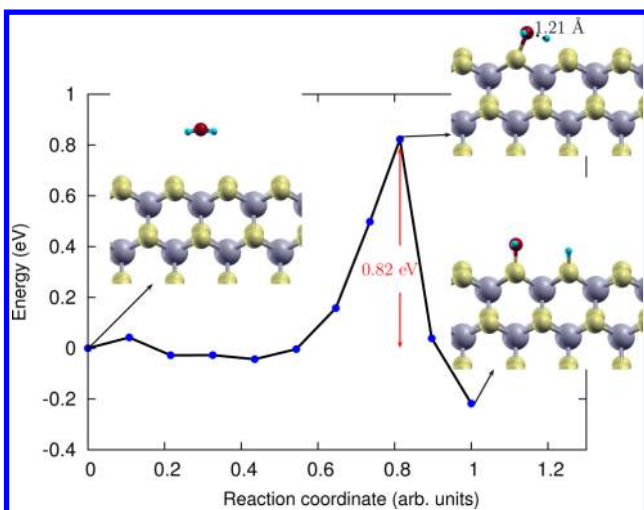
Figure 5. Reaction pathway and reaction barrier of single water dissociation on S50-edge from climbing image nudged elastic band (CI-NEB) simulation. Purple atoms represent Mo; yellow atoms represent S.
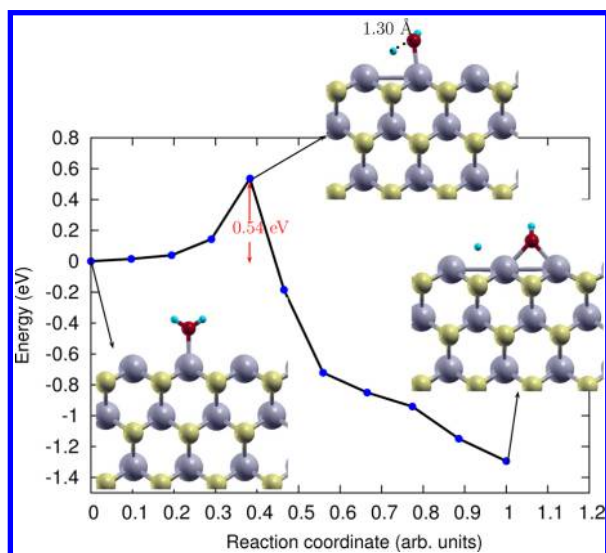

Figure 6. Reaction pathway and reaction barrier of single water dissociation on Mo-edge from climbing image nudged elastic band (CI-NEB) simulation. Purple atoms represent Mo; yellow atoms represent S.

MEP. All the reaction paths were found to have similar TSs where the H_2O molecule has dissociated into OH and H species; the OH group has bonded to a surface atom for all the edges, while the H atom has bonded to a surface atom for the S100-edge but remains unbonded for the remaining two edges. Eventually the H atoms draw close to the surface and form bonds in the FS for each edge. For the Mo-edge FS, the H atom remains in a position roughly equidistant between two adjacent surface Mo atoms, which suggests it shares bonds with both surface atoms. For the two S-edges, the H atoms form bonds with a single surface atom in the FS configurations.

The TSs can be used to find the activation energies for the dissociation reaction at ground state conditions. The activation energy barrier is defined as $E_a = E_{TS} - E_{IS}$, where E_{TS} is the energy of the transition state and E_{IS} is the energy of the IS. The calculated activation energy barrier E_a for water dissociation on S100-edge had a relatively high value of 2.31

eV. The S50-edge had a significantly lower barrier of 0.82 eV while the Mo-edge had the lowest barrier at 0.54 eV. The activation energy barriers for all the edges were significantly lower than that for water splitting in free space (~5 eV). The energy barriers for S50-edge and Mo-edge were even lower than water splitting in liquid water (~1 eV)[44,45] and on the surfaces of Cu, Ni, and Pd (~1 eV).[1] The activation energy barrier for water splitting on Mo-edge was comparable with that of water dissociation over a semiconducting (8,0) CNT (~0.48 eV) and on a metallic (5,5) CNT (~0.41 eV).[46] In particular, this compares favorably with platinum surface, which is often regarded as the best performing catalyst for such reactions. A recent DFT based study found a minimum activation energy of 0.44 eV for Pt(110) surface but higher than 0.54 eV for the other four crystal surfaces tested.[29] Thus, the magnitude of the activation barriers for the S50-edge and Mo-edge can likely be overcome with relatively low energy inputs (thermal, electric, or photonic).

The reaction energy is defined as $\Delta E = E_{FS} - E_{IS}$, where E_{FS} is the energy of the FS, so that a negative ΔE indicates an exothermic reaction and a positive ΔE represents an endothermic one. The H_2O dissociation on S100-edge was endothermic with positive reaction energy difference of 1.4 eV (Figure 4). On the other hand, both S50-edge (Figure 5) and Mo-edge (6) had exothermic negative reaction energies of −0.22 and −1.29 eV, respectively. This beats the best reaction energy obtained for Pt surfaces with a figure of −0.20 eV.[29] The much larger magnitude of the Mo-edge reaction energy in relation to the S-edges is likely in relation to its superior water adsorption ability, whereas the S-edges did not even favorably adsorb H_2O molecules in their ISs. The negative reaction energies for the Mo-edge and S50-edge point to thermodynamic favorably, and the low activation barriers point to favorable kinetics. On the other hand, water dissociation on the S100-edge is energetically less favorable due to its comparatively higher activation barrier and large positive reaction energy, and thus the S100-edge is not a good candidate for water splitting.

3.3. Free Energy of Water Dissociation on Mo-Edge at Room Temperature with Vibrational and Entropic Contributions. Although NEB analysis revealed the Mo-edge as highly active for water dissociation, the reaction energy results only provided potential energy differences at ground state. In order to get a more complete picture of behavior under room temperature conditions for the best performing Mo-edge, we considered quantum corrections to the activation barrier in order to account for the discreteness of vibrational modes at room temperature (300 K). Therefore, the entropic contribution as well as zero point energy (ZPE) correction were incorporated by computing Gibbs free energy ΔG_a between IS and TS, such that

$$\Delta G_a = E_a + \Delta ZPE - T\Delta S \qquad (2)$$

where E_a is activation energy barrier obtained by subtracting total energies of IS and TS as defined in section 3.2 and obtained from NEB, ΔZPE is the difference of zero point energies between IS and TS, ΔS is the change of entropy of water between IS and TS, and T is the temperature. The ΔZPE was computed to be −0.404 eV through the vibrational frequency calculation.

The entropic contribution ($T\Delta S$) can be considered to be very low for adsorbate species as they are already bound to a surface with little configurational freedom.[47] Typically, the
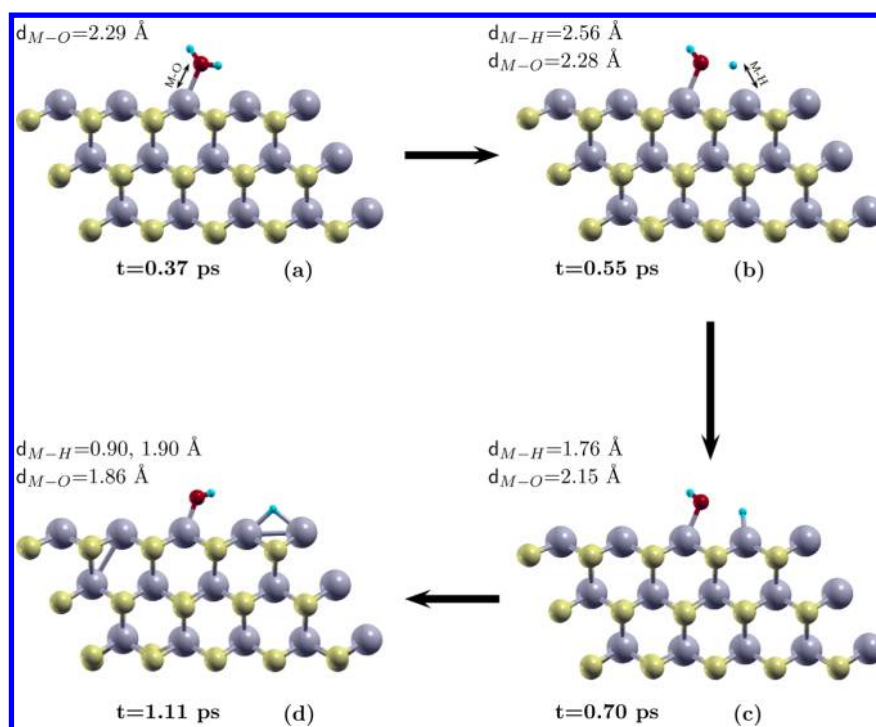
Figure 7. Reaction mechansim of H_2O dissociation reaction on Mo-edge of MoS_2 during unbiased *ab initio* molecular dynamics simulation at 300 K. The reaction roughly follows the same path as CI-NEB simulations.

entropy of adsorbed molecules is almost entirely in the vibrational partition with little translational or rotational contributions, with most of the freedom related to vibration of the molecule normal to the surface and so largely dependent on bond length and strength between between adsorbate and surface.[48] For the Mo-edge, both the water molecule in the IS and OH species in the TS are bound to the surface at similar distances (2.23 and 2.12 Å, respectively) and can be considered to have zero entropy difference. The dissociated H atom in the TS might produce an entropy difference depending on how strongly it is bound to the surface; if it is considered to have strong adsorption like the other species, then the entropy difference remains zero ($T\Delta S = 0$). An upper bound for the entropy difference term can be obtained if the H atom in the TS is considered to be fully free of the surface and act as a free gas, in which case the $T\Delta S$ value is 0.20 eV/H_2O at room temperature.[47] After considering these corrections, we calculated the free energy change ΔG_a of activation for the reaction to be from 0.14 eV ($T\Delta S = 0$) to −0.06 eV ($T\Delta S = 0.20$) on Mo-edge which suggests not only that the Mo-edge has excellent catalytic activity but also that water dissociation on Mo-edge could be spontaneous at finite temperature, making it a defect-free alternative to oxygen vacant MoS_2 surface suggested by Ataca et al.[24] for dissociating H_2O spontaneously. The kinetic rate constant can be estimated by the transition state theory expression

$$k = \frac{k_B T}{h} \exp(-\Delta G_a/k_B T) \tag{3}$$

where k_B and h denote Boltzmann's and Planck's constant, respectively. From the formula above, we determined a range for the rate constant from $k = 2.8 \times 10^{10}$ s^{-1} ($T\Delta S = 0$) to $k = 6.4 \times 10^{13}$ s^{-1} ($T\Delta S = 0.14$) at 300 K. A change of 0.06 eV in activation barrier produces an approximate rise or fall in reaction rate by 1 order of magnitude. However, even with a

few orders of magnitude change in value, this would still be a very high rate constant. This clearly suggests that the Mo-edge is very favorable for the water dissociation reaction not only thermodynamically but also kinetically, and the reaction is likely to occur spontaneously and quickly at room temperature. Hence, water dissociation is likely not the rate-limiting step as part of an overall hydrogen evolution process; we studied further steps in section 3.6.

3.4. Finite Temperature *ab Initio* Molecular Dynamics. Water dissociation on the Mo-edge, the best performing of the MoS_2 surfaces, was selected for finite temperature AIMD simulations to observe temperature effects on the dynamic evolution of the system. The system was initialized with the H_2O molecule oriented so as to have the O atom facing the MoS_2 surface and then allowed to evolve along the Born–Oppenheimer energy surface at 300 K. As the simulation progressed, the H_2O molecule started to move toward the MoS_2 surface and tilt to allow the O atom to decrease its distance to the nearest Mo atom and eventually started to form a bond between the O and Mo atoms (see Figure 7a) at $t \simeq$ 0.37 ps in the dynamics. Next, one of the H atoms in the H_2O molecule started to detach from the O atom (Figure 7b) and form a bond with the Mo atom adjacent to the O bonded Mo atom (Figure 7c). By $\simeq$ 1.11 ps, the first detached H atom had moved to a position intermediate between two Mo atoms and seemed to form bonds with both of them, achieving a configuration similar to that observed for the adsorption simulations in section 3.1 (see Figure 7d). This configuration continued to be stable for the remaining simulation time up to 1.48 ps, at which point the simulation was stopped as complete dissociation had been achieved and there was little change in the atomic configurations.

The quick and straightforward dissociation of the H_2O molecule into OH and H in under 1.5 ps indicates that the energy barrier for dissociation is not larger than the thermal
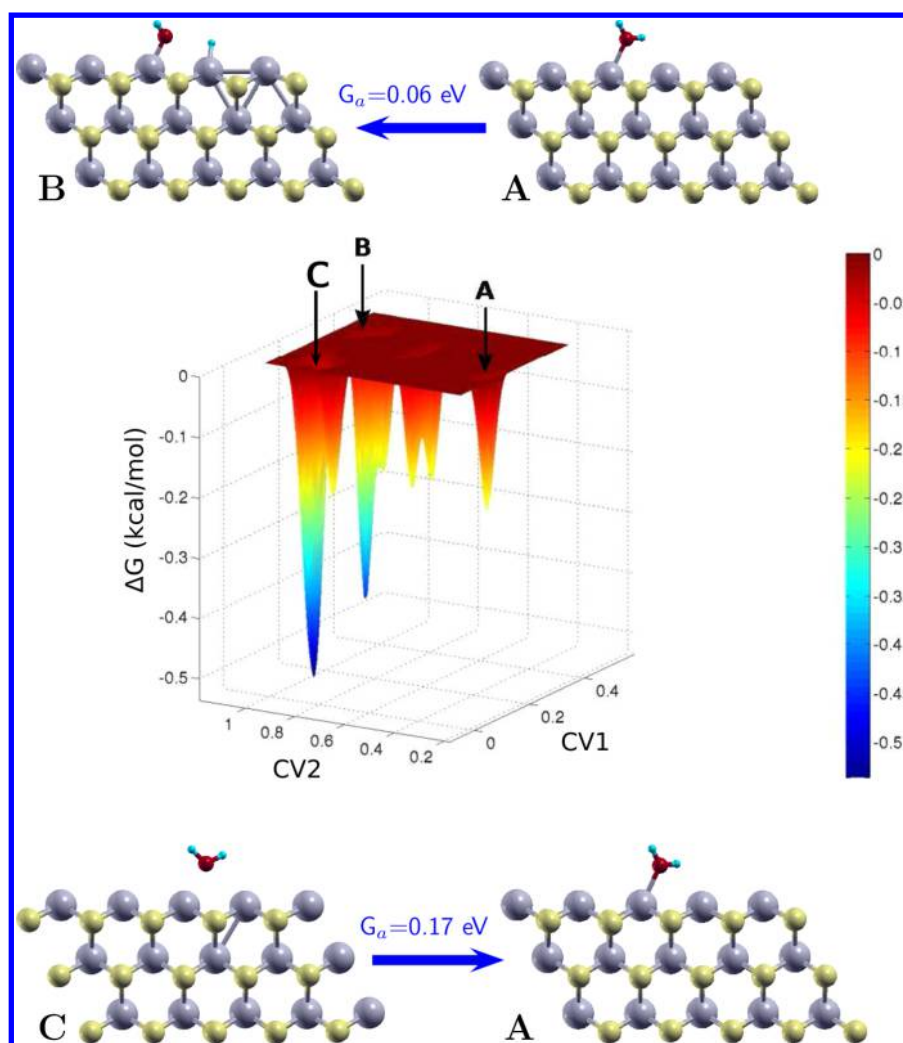
Figure 8. Free energy surface of mechanism 1 in terms of collective variables for metadynamics biased AIMD simulation at 300 K and 2.5 fs time step with corresponding atomic configurations at specific energy minima. The dissociation reaction proceeds from point A to B. However, the deepest energy well and largest activation barrier correspond to adsorption of the free water molecule at point C. The activation energy barriers G_a, obtained from 1.25 fs time step simulations, are given in blue.

energy available at 300 K. This confirms the spontaneous nature of H_2O molecule dissociation on the Mo-edge surface and that it strongly favors this reaction even at room temperature. This also correlates with the earlier calculated rate constants as it falls within the range of prediction of a dissociation happening once every 0.02−36.0 ps on average, with it falling closer to the lower bound which corresponds to a TS with a free H atom and bound OH species. The initial H_2O adsorption took place at the same active site found as most favorable in the adsorption simulations (marked Mo1 in Figure 2c). The overall evolution of the reaction was also found to be similar to the adsorption and NEB based results, especially the final configuration of the dissociated water molecule. In both approaches, the O atoms first forms a bond to the nearest Mo atom while the H_2O molecule is still intact. The first H atom to detach from the water molecule stabilizes roughly intermediate between two Mo atoms in both the AIMD and adsorption results. Hence, the dissociation proceeds in a roughly similar manner even with entropic and temperature effects.

3.5. Metadynamics Biased Finite Temperature *ab Initio* Molecular Dynamics. The water dissociation AIMD simulation conducted on the Mo-edge in section 3.4 was

repeated with a metadynamics based bias and the same time step of 2.5 fs in order to obtain a free energy surface of the reaction and explore possible alternate reaction mechanisms. Two schemes of collective variables were tested in two different biased simulations, and each resulted in a different reaction mechanism, both of which are presented in the following sections. Once an energy surface was obtained for a mechanism, specific regions of the surface corresponding to important energy barriers were explored with a smaller time step of 1.25 fs in order to obtain a more detailed and accurate estimate of free energy barriers, and these values are presented in the following sections.

3.5.1. Mechanism 1. In the first simulation scheme, two collective variables were biased, the first (CV1) representing coordination number between the O atom in the H_2O molecule and the nearest Mo atom and the second (CV2) representing coordination number between the O atom in the H_2O molecule and a H atom in the same molecule (see Supporting Information for coordination number collective variable definitions). The reaction proceeds according to the same mechanism as found from NEB and the unbiased AIMD simulations; namely, the H_2O molecule dissociates into OH
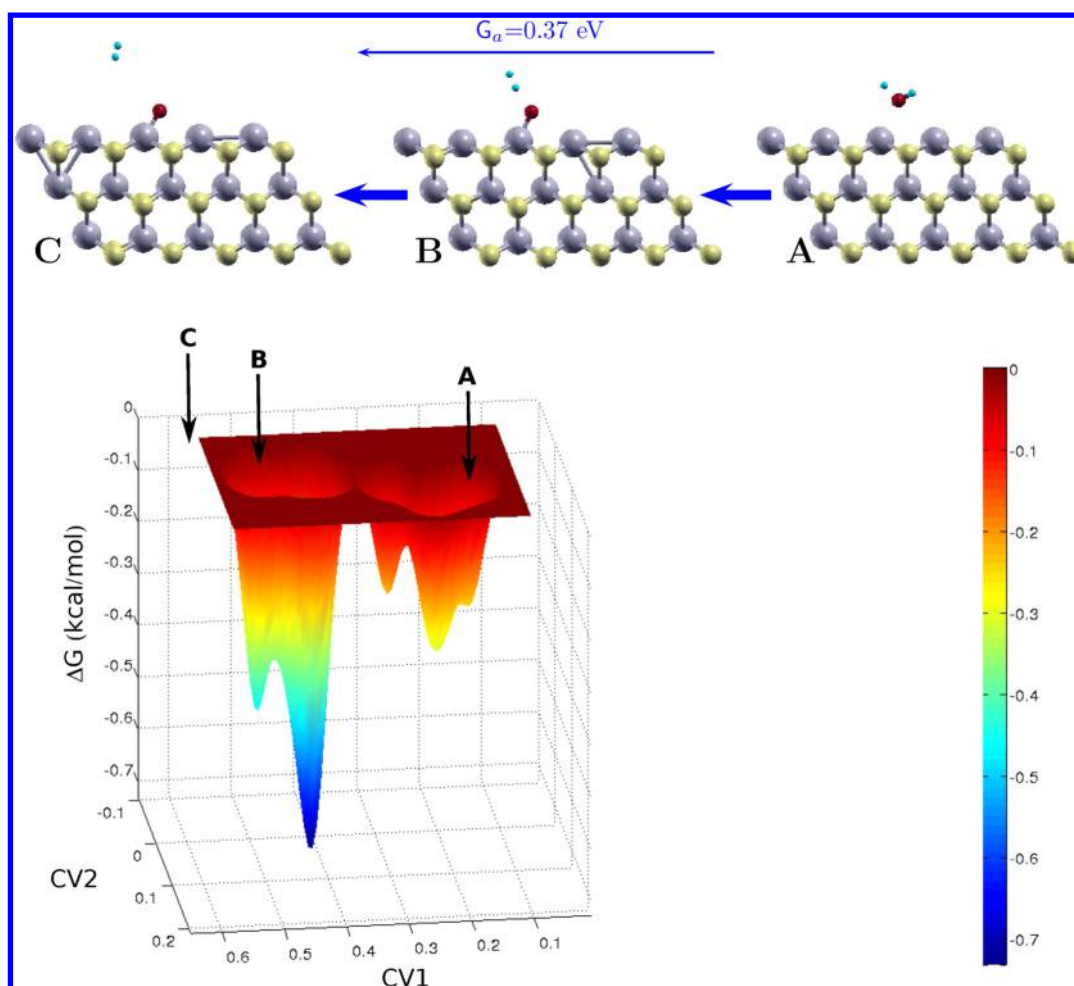
Figure 9. Free energy surface of mechanism 2 in terms of collective variables for metadynamics biased AIMD simulation at 300 K 2.5 fs time step with corresponding atomic configurations at specific energy minima. The dissociation reaction proceeds from point A to B and then C, leaving behind a lone adsorbed O atom. The activation energy barrier G_a for the overall process, obtained from 1.25 fs time step simulations, is given in blue.

and H species which both adsorb on Mo atoms on the Mo-edge surface. During the dissociation, the H_2O molecule's O atom first forms a bond with a Mo atom and then a H atom splits from the molecule, leaving the OH species adsorbed, and eventually the H also adsorbs to surface Mo atoms. The resulting free energy surface is described in Figure 8.

The free energy minima corresponding to the IS (representing the adsorbed H_2O molecule) and FS (representing adsorbed OH and H) from the NEB simulations are labeled A and B, respectively. The free energy barrier for escaping from the energy well at A, which corresponds to an activation energy barrier, is roughly 0.06 eV (5.89 kJ/mol). This value falls within the range of free energy barriers calculated from the NEB calculations (−0.06 to 0.14 eV) and lies closer to the lower bound which was associated with the intermediate transition state (TS) consisting of a bound OH and free H atom (while the upper bound consisted of both OH and H species bound to the surface with practically no freedom of movement). This also matches the results of the nonbiased AIMD simulation in which the dissociation also happened with a time closer to that predicted by the lower bound barrier. Hence, the TS probably has an H atom loosely attracted to and held by the surface which is not fully adsorbed and possess more freedom of movement than the final bound state but less than in free gas state. The free energy surface also confirms that the water

dissociation step is not the rate-limiting step in the overall water to hydrogen process as it does not involve the deepest energy well labeled as C in Figure 8. Instead, the deepest energy well represents the unadsorbed free water molecule, and the free energy barrier for escaping from this well (corresponding to water adsorption on the surface) is 0.17 eV (16.40 kJ/mol). This demonstrates that, even for the Mo-edge which is thermodynamically favorable for water adsorption, the water adsorption step is a candidate for the rate-limiting step for the hydrogen production process.

3.5.2. Mechanism 2. The second biased simulation scheme also utilized two collective variables: the first (CV1) representing coordination number between the O atom in the H_2O molecule and the nearest two surface Mo atoms and the second (CV2) representing coordination number between an H atom and the two nearest Mo atoms to which it was bound in the final state of the unbiased AIMD simulation. The dissociation of this reaction proceeded by a different mechanism than for the first biased simulation scheme. The common process for generation of hydrogen from water on catalyst surfaces involves water splitting into adsorbed H and OH ($H_2O + 2* \rightarrow OH* + H*$, where * represents a surface site), as was the case for our NEB and AIMD simulations. The adsorbed hydrogens eventually combine to form a hydrogen molecule (through the simple route $2H* \rightarrow H_2$ or more

complex intermediates), leaving behind the adsorbed OH species.[47] However, an alternate mechanism involves the hydrogen atoms of the water molecule directly combing to form a hydrogen molecule while leaving behind only the O atom adsorbed ($H_2O + * \rightarrow O* + H_2$), which seems to be the mechanism followed by the second simulation scheme.

Figure 9 describes the free energy surface for this simulation. The free energy minima corresponding to the unadsorbed whole water molecule is labeled A. The O atom proceeds to adsorb strongly to the nearest Mo atom while the H atoms are starting to break free of the O atom by point B. At point C, the two H atoms have fully broken away from the O atom and are moving away from the MoS_2 surface while drawing closer to each other to form what looks like an H_2 molecule. The free energy barrier for the H atoms to escape the O atom and go from point B to C was roughly 0.36 eV (34.74 kJ/mol). This is significantly higher than the energy barrier for breaking the O−H bond in mechanism 1, which is to be expected as there now two bonds being broken at roughly the same time. Hence, this mechanism will occur far less frequently than mechanism 1 at room temperature. However, the activation barrier is not particularly high and can be overcome with a slight energy input. It should be noted that the barrier is also greater than that for water adsorption in mechanism 1.

3.6. Surface Processes Subsequent to Water Dissociation. Following the splitting of the water molecule into OH and H species in mechanism 1, there are several additional steps required for hydrogen gas production. A preliminary examination of these on the Mo-edge was done by studying the further dissociation of the OH species into O and H, the migration of H atoms across the Mo-edge surface, and the possible formation of hydrogen by the simple route of the Tafel reaction ($2H* \rightarrow H_2$) at ground state conditions. The OH splitting reaction ($OH* \rightarrow H* + O*$) was found to be thermodynamically favorable with a reaction energy ΔE of −1.58 eV but had a significant activation energy E_a of 2.00 eV (see Supporting Information for geometrical configurations of this reaction). The ΔE for OH dissociation compares very favorably with other metals such as Au, Cu, Pt, and Pd which have either endothermic or thermoneutral reaction energies[1] but smaller activation energies ranging from 0.96 to 1.79 eV.

The intermediate states for H atom migration, association, and desorption from the Mo-edge, along with their relative energies, are shown in Figure 10. First, two distant (out of each other's bonding range) surface bonded H atoms were made to move toward each other. The intermediate state for this process, corresponding to an H atom between and not strongly bound to adjacent Mo atoms, produced an activation barrier E_a of 1.15 eV for H migration. Eventually the two H atoms moved close enough to be bonded to the same Mo atom, a configuration which had a lower energy than the initial state in which the H atoms were far apart. The desorption of the two adjacent H atoms to then form an H_2 molecule was found to have an equivalent E_a and ΔE of 1.07 eV, indicating there is not an intermediate highest energy transition state. The activation energy for these postdissociation processes are higher than that for the water splitting step, hinting that one of these steps is likely the rate-limiting step for a full hydrogen evolution reaction. The hydrogen desorption step is especially troublesome as even the overall reaction seems to be thermodynamically unfavorable with a positive potential energy change. However, it should also be noted that for desorption processes, where the gas phase transition or final state can have
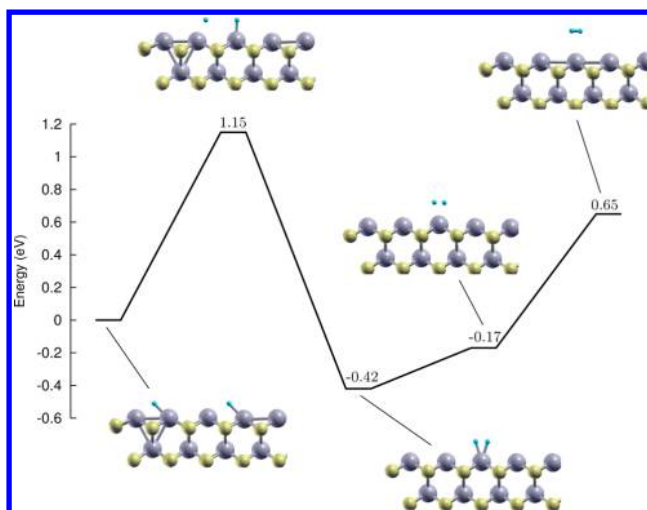

Figure 10. Intermediate states for the process of H atom migration, association, and desorption from Mo-edge. The energy difference, ΔE, for each state relative to the initial configuration of separated and adsorbed individual H atoms is provided.

significantly greater freedom of movement than the initial adsorbed state, entropy can be a significant factor and greatly lower the free energy of activation or reaction for the step.[48] Furthermore, the hydrogen evolution step might proceed by a more complex route with several intermediate species than the simple Tafel mechanism tested.

The preliminary simulations demonstrate that the hydrogen desorption mechanism needs to be studied in greater detail with finite temperature entropy effects and exploration of multiple possible reaction pathways. Additionally, this work was restricted to studying a single H_2O molecule on the edge surface and did not consider the impact of multiple H_2O molecules. Other H_2O molecules can affect reaction mechanisms due to their polar nature, although this is much more significant in liquid phase reactions where they can protonate H atoms. Another important factor for surface catalytic reactions involves surface coverage effects where adsorbed molecules can interact with each other and even form surface layers. Surface layers themselves can interfere with adsorption of reactants and affect reaction rates. This also brings up the issue of the O atom which is left adsorbed to the surface and whether it is removed by some reaction such as O_2 evolution; otherwise, this might result in the poisoning of the catalytic surface. Such considerations will have to be properly investigated before the MoS_2 monolayer material can be used for practical applications. As such, these should be explored in future studies.

4. CONCLUSION

The water adsorption and dissociation abilities of three edge terminations of monolayer MoS_2 with 100% sulfur (S) coverage (S100-edge), 50% S coverage (S50-edge), and 0% S coverage (Mo-edge) were investigated using *ab initio* simulations. The S100 and S50 edges were found to be thermodynamically unfavorable for H_2O adsorption while all edges were able to strongly bind the individual OH and H species on their surface. Next, water dissociation was simulated for all edges using the nudged elastic band (NEB) method. All edges followed roughly the same reaction path, during which an H atom split from the H_2O molecule to leave an adsorbed OH and eventually

adsorbed itself onto the surface. The S100-edge turned out to have a very high ground state activation energy barrier of 2.31 eV, while the S50-edge had a barrier of 0.82 eV and the Mo-edge had the lowest barrier of 0.54 eV. The Mo-edge activation free energy barrier was then found using zero-point energy and entropy corrections to produce a barrier in the range of −0.06 to 0.14 eV and a very high rate constant which indicated that the water dissociation reaction would proceed spontaneously on the Mo-edge at room temperature.

Water dissociation was then further studied on the Mo-edge using *ab initio* molecular dynamics with metadynamics to study the reaction when the system was allowed to evolve freely at finite temperature with no fixed final state. Water splitting occurred through two mechanisms. Mechanism 1 followed the mechanism of the NEB simulations and produced a dissociation activation free energy barrier of 0.06 eV. It was also found that the water adsorption step for mechanism 1 had a higher activation free energy barrier of 0.17 eV than for water dissociation. Mechanism 2 occurred via a pathway in which the H atoms of the H_2O molecule directly form a hydrogen molecule while leaving behind an adsorbed O atom and had a higher activation free energy barrier of 0.36 eV. Finally, steps required for hydrogen evolution after water dissociation were studied for the Mo-edge. The dissociation of OH was found to have a ground state activation energy barrier of 2.00 eV, H atom migration on the surface was found to have a barrier of 1.15 eV, and the association and desorption of H_2 was found to have a barrier of 1.07 eV. Hence, it was found that water dissociation is likely not the rate-limiting step for hydrogen production on MoS_2 edges.

ASSOCIATED CONTENT

Ⓢ Supporting Information

MoS_2 model structural and electronic property validation, Bader charge analysis for H_2O adsorption, metadynamics simulations details. This material is available free of charge via the Internet at http://pubs.acs.org.

AUTHOR INFORMATION

Corresponding Author

*Fax +1 416 978 4155; Tel +1 416 946 5211; e-mail chandraveer.singh@utoronto.ca (C.V.S.).

Notes

The authors declare no competing financial interest.

ACKNOWLEDGMENTS

REFERENCES

(1) Phatak, A. A.; Delgass, W. N.; Ribeiro, F. H.; Schneider, W. F. Density Functional Theory Comparison of Water Dissociation Steps on Cu, Au, Ni, Pd, and Pt. *J. Phys. Chem. C* **2009**, *113*, 7269−7276.

(2) Kudo, A.; Miseki, Y. Heterogeneous Photocatalyst Materials for Water Splitting. *Chem. Soc. Rev.* **2009**, *38*, 253−278.

(3) Sandhya, K. S.; Suresh, C. H. Designing Metal Hydride Complexes for Water Splitting Reactions: A Molecular Electrostatic Potential Approach. *Dalton Trans.* **2014**, *43*, 12279−12287.

(4) Kang, J.; Tongay, S.; Zhou, J.; Li, J.; Wu, J. Band Offsets and Heterostructures of Two-Dimensional Semiconductors. *Appl. Phys. Lett.* **2013**, *102*, 012111.

(5) Tongay, S.; Zhou, J.; Ataca, C.; Lo, K.; Matthews, T. S.; Li, J.; Grossman, J. C.; Wu, J. Thermally Driven Crossover from Indirect toward Direct Bandgap in 2D Semiconductors: $MoSe_2$ versus MoS_2. *Nano Lett.* **2012**, *12*, 5576−5580.

(6) Coleman, J. N.; Lotya, M.; O'Neill, A.; Bergin, S. D.; King, P. J.; Khan, U.; Young, K.; Gaucher, A.; De, S.; Smith, R. J.; et al. Two-Dimensional Nanosheets Produced by Liquid Exfoliation of Layered Materials. *Science* **2011**, *331*, 568−571.

(7) Ataca, C.; Sahin, H.; Ciraci, S. Stable, Single-Layer MX_2 Transition-Metal Oxides and Dichalcogenides in a Honeycomb-Like Structure. *J. Phys. Chem. C* **2012**, *116*, 8983−8999.

(8) Li, T.; Galli, G. Electronic Properties of MoS_2 Nanoparticles. *J. Phys. Chem. C* **2007**, *111*, 16192−16196.

(9) Schweiger, H.; Raybaud, P.; Kresse, G.; Toulhoat, H. Shape and Edge Sites Modifications of MoS_2 Catalytic Nanoparticles Induced by Working Conditions: A Theoretical Study. *J. Catal.* **2002**, *207*, 76−87.

(10) Ataca, C.; Şahin, H.; Aktürk, E.; Ciraci, S. Mechanical and Electronic Properties of MoS_2 Nanoribbons and Their Defects. *J. Phys. Chem. C* **2011**, *115*, 3934−3941.

(11) Ataca, C.; Topsakal, M.; Akturk, E.; Ciraci, S. A Comparative Study of Lattice Dynamics of Three- and Two-Dimensional MoS_2. *J. Phys. Chem. C* **2011**, *115*, 16354−16361.

(12) Bernardi, M.; Palummo, M.; Grossman, J. C. Extraordinary Sunlight Absorption and 1 nm-Thick Photovoltaics Using Two-Dimensional Monolayer Materials. *Nano Lett.* **2013**, *13*, 3664−3670.

(13) Yun, W. S.; Han, S. W.; Hong, S. C.; Kim, I. G.; Lee, J. D. Thickness and Strain Effects on Electronic Structures of Transition Metal Dichalcogenides: 2H-MX_2 Semiconductors (M = Mo, W; X = S, Se, Te). *Phys. Rev. B* **2012**, *85*, 033305.

(14) Ding, Y.; Wang, Y.; Ni, J.; Shi, L.; Shi, S.; Tang, W. First Principles Study of Structural, Vibrational and Electronic Properties of Graphene-Like {MX_2} (M = Mo, Nb, W, Ta; X = S, Se, Te) Monolayers. *Physica B* **2011**, *406*, 2254−2260.

(15) Min, Y.; He, G.; Xu, Q.; Chen, Y. Dual-Functional MoS_2 Sheet-Modified CdS Branch-Like Heterostructures with Enhanced Photostability and Photocatalytic Activity. *J. Mater. Chem. A* **2014**, *2*, 2578−2584.

(16) Jaegermann, W.; Tributsch, H. Interfacial Properties of Semiconducting Transition Metal Chalcogenides. *Prog. Surf. Sci.* **1988**, *29*, 1−167.

(17) Lauritsen, J. V.; Kibsgaard, J.; Helveg, S.; Topsoe, H.; Clausen, B. S.; Laegsgaard, E.; Besenbacher, F. Size-Dependent Structure of MoS_2 Nanocrystals. *Nat. Nanotechnol.* **2007**, *2*, 53−58.

(18) Jaramillo, T. F.; Jorgensen, K. P.; Bonde, J.; Nielsen, J. H.; Horch, S.; Chorkendorff, I. Identification of Active Edge Sites for Electrochemical H_2 Evolution from MoS_2 Nanocatalysts. *Science* **2007**, *317*, 100−102.

(19) Hinnemann, B.; Moses, P. G.; Bonde, J.; Jorgensen, K. P.; J. H. Nielsen, I. C.; Horch, S.; Norskov, J. K. Biomimetic Hydrogen Evolution: MoS_2 Nanoparticles as Catalyst for Hydrogen Evolution. *J. Am. Chem. Soc.* **2005**, *127*, 5308−5309.

(20) Li, Y.; Wang, H.; Xie, L.; Liang, Y.; Hong, G.; Dai, H. MoS_2 Nanoparticles Grown on Graphene: An Advanced Catalyst for the Hydrogen Evolution Reaction. *J. Am. Chem. Soc.* **2011**, *133*, 7296−7299.

(21) Bonde, J.; Moses, P. G.; Jaramillo, T. F.; Norskov, J. K.; Chorkendorff, I. Hydrogen Evolution on Nano-Particulate Transition Metal Sulfides. *Faraday Discuss.* **2009**, *140*, 219−231.

(22) Kibsgaard, J.; Chen, Z.; Reinecke, B. N.; Jaramillo, T. F. Engineering the Surface Structure of MoS₂ to Preferentially Expose Active Edge Sites for Electrocatalysis. *Nat. Mater.* **2012**, *11*, 963−969.

(23) Chung, D. Y.; Park, S.-K.; Chung, Y.-H.; Yu, S.-H.; Lim, D.-H.; Jung, N.; Ham, H. C.; Park, H.-Y.; Piao, Y.; Yoo, S. J.; et al. Edge-Exposed MoS₂ Nano-Assembled Structures as Efficient Electrocatalysts for Hydrogen Evolution Reaction. *Nanoscale* **2014**, *6*, 2131−2136.

(24) Ataca, C.; Ciraci, S. Dissociation of H₂O at the Vacancies of Single-Layer MoS₂. *Phys. Rev. B* **2012**, *85*, 195410.

(25) Raybaud, P.; Hafner, J.; Kresse, G.; Kasztelan, S.; Toulhoat, H. Ab Initio Study of the H₂-H₂S/MoS₂ Gas-Solid Interface: The Nature of the Catalytically Active Sites. *J. Catal.* **2000**, *189*, 129−146.

(26) Shi, X.; Wang, S.; Hu, J.; Wang, H.; Chen, Y.; Qin, Z.; Wang, J. Density Functional Theory Study on Water-Gas-Shift Reaction over Molybdenum Disulfide. *Appl. Catal., A* **2009**, *365*, 62−70.

(27) Chen, Y.-Y.; Dong, M.; Wang, J.; Jiao, H. On the Role of a Cobalt Promoter in a Water-Gas-Shift Reaction on Co-MoS₂. *J. Phys. Chem. C* **2010**, *114*, 16669−16676.

(28) Chen, Y.-Y.; Dong, M.; Wang, J.; Jiao, H. Mechanisms and Energies of Water Gas Shift Reaction on Fe-, Co-, and Ni-Promoted MoS₂ Catalysts. *J. Phys. Chem. C* **2012**, *116*, 25368−25375.

(29) Fajin, J. L. C.; D.S.Cordeiro, M. N.; Gomes, J. R. B. Density Functional Theory Study of the Water Dissociation on Platinum Surfaces: General Trends. *J. Phys. Chem. A* **2014**, *118*, 5832−5840.

(30) Fajin, J. L. C.; Cordeiro, M. N. D. S.; Illas, F.; Gomes, J. R. B. Descriptors Controlling the Catalytic Activity of Metallic Surfaces toward Water Splitting. *J. Catal.* **2010**, *276*, 92−100.

(31) Fajin, J. L. C.; Cordeiro, M. N. D. S.; Illas, F.; Gomes, J. R. B. Influence of Step Sites in the Molecular Mechanism of the Water Gas Shift Reaction Catalyzed by Copper. *J. Catal.* **2009**, *268*, 131−141.

(32) Gokhale, A.; Dumesic, J. A.; Mavrikakis, M. On the Mechanism of Low-Temperature Water Gas Shift Reaction on Copper. *J. Am. Chem. Soc.* **2008**, *130*, 1402−1414.

(33) Giannozzi, P.; Baroni, S.; Bonini, N.; Calandra, M.; Car, R.; Cavazzoni, C.; Ceresoli, D.; Chiarotti, G.; Cococcioni, M.; Dabo, I.; et al. Quantum Espresso: A Modular and Open-Source Software Project for Quantum Simulations of Materials. *J. Phys.: Condens. Matter* **2009**, *21*, 395502.

(34) Kresse, G.; Joubert, D. From Ultrasoft Pseudopotentials to the Projector Augmented-Wave Method. *Phys. Rev. B* **1999**, *59*, 1758−1775.

(35) Perdew, J. P.; Burke, K.; Ernzerhof, M. Generalized Gradient Approximation Made Simple. *Phys. Rev. Lett.* **1996**, *77*, 3865−3868.

(36) Monkhorst, H. J.; Pack, J. D. Special Points for Brillouin-Zone Integrations. *Phys. Rev. B* **1976**, *13*, 5188−5192.

(37) Lee, K.; Murray, E. D.; Kong, L.; Lundqvist, B. I.; Langreth, D. C. Higher-Accuracy van der Waals Density Functional. *Phys. Rev. B* **2010**, *82*, 081101.

(38) Mills, G.; Jonsson, H.; Schenter, G. K. Reversible Work Transition State Theory: Application to Dissociative Adsorption of Hydrogen. *Surf. Sci.* **1995**, *324*, 305−337.

(39) Jónsson, H.; Mills, G.; Jacobsen, K. W. *Classical and Quantum Dynamics in Condensed Phase Simulations*; World Scientific: Singapore, 1998; Chapter 16, pp 385−404.

(40) Henkelman, G.; Jonsson, H. G. Improved Tangent Estimate in the Nudged Elastic Band Method for Finding Minimum Energy Paths and Saddle Points. *J. Chem. Phys.* **2000**, *113*, 9978.

(41) Laio, A.; Parrinello, M. Escaping Free-Energy Minima. *Proc. Natl. Acad. Sci. U. S. A.* **2002**, *99*, 12562−12566.

(42) Laio, A.; Gervasio, F. L. Metadynamics: A Method to Simulate Rare Events and Reconstruct the Free Energy in Biophysics, Chemistry and Material Science. *Rep. Prog. Phys.* **2008**, *71*, 126601.

(43) Tribello, G. A.; Bonomi, M.; Branduardi, D.; Camilloni, C.; Bussi, G. {PLUMED} 2: New Feathers for an Old Bird. *Comput. Phys. Commun.* **2014**, *185*, 604−613.

(44) Henderson, M. A. The Interaction of Water with Solid Surfaces: Fundamental Aspects Revisited. *Surf. Sci. Rep.* **2002**, *46*, 1−308.

(45) Kostov, M. K.; Santiso, E. E.; George, A. M.; Gubbins, K. E.; Nardelli, M. B. Dissociation of Water on Defective Carbon Substrates. *Phys. Rev. Lett.* **2005**, *95*, 136105.

(46) Lei, Y.; Guo, Z. X.; Zhu, W.; Meng, S.; Zhang, Z. Initial Interactions Between Water Molecules and Ti-Adsorbed Carbon Nanotubes. *Appl. Phys. Lett.* **2007**, *91*, 161906−161906−3.

(47) Norskov, J. K.; Bligaard, T.; Logadottir, A.; Kitchin, J. R.; Chen, J. G.; Pandelov, S.; Stimming, U. Trends in the Exchange Current for Hydrogen Evolution. *J. Electrochem. Soc.* **2005**, *152* (3), J23−J26.

(48) van Santen, R. A.; Neurock, M. *Principles of Molecular Heterogeneous Catalysis*; Wiley-VCH Verlag GmbH and Co. KGaA: Weinheim, 2007; pp 19−81.

(49) Loken, C.; Gruner, D.; Groer, L.; Peltier, R.; Bunn, N.; Craig, M.; Henriques, T.; Dempsey, J.; Yu, C.-H.; Chen, J.; et al. SciNet: Lessons Learned from Building a Power-efficient Top-20 System and Data Centre. *J. Phys. Conf. Ser.* **2010**, *256*, 012026.